Anomalous Tunneling in Carbon/Alkane/TiO_2/Gold Molecular Electronic Junctions: Energy Level Alignment at the Metal/Semiconductor Interface

Haijun Yan[†,‡] and Richard L. McCreery*[,‡,§]

Department of Chemistry, The Ohio State University, 100 West 18th Avenue, Columbus, Ohio 43210, National Institute for Nanotechnology, National Research Council of Canada, Edmonton, Alberta, Canada T6G 2M9, and Department of Chemistry, University of Alberta, Edmonton, Alberta, Canada T6G 2G2

ABSTRACT Carbon/TiO_2/gold electronic junctions show slightly asymmetric electronic behavior, with higher current observed in current density (*J*)/voltage (*V*) curves when carbon is biased negative with respect to the gold top contact. When a ~1-nm-thick alkane film is deposited between the carbon and TiO_2, resulting in a carbon/alkane/TiO_2/gold junction, the current increases significantly for negative bias and decreases for positive bias, thus creating a much less symmetric *J*/*V* response. Similar results were obtained when SiO_2 was substituted for the alkane layer, but Al_2O_3 did not produce the effect. The observation that, by the addition of an insulating material between carbon and TiO_2, the junction becomes more conductive is unexpected and counterintuitive. Kelvin probe measurements revealed that while the apparent work function of the pyrolyzed photoresist film electrode is modulated by surface dipoles of different surface-bound molecular layers, the anomalous effect is independent of the direction of the surface dipole. We propose that by using a nanometer-thick film with a low dielectric constant as an insertion layer, most of the applied potential is dropped across this thin film, thus permitting alignment between the carbon Fermi level and the TiO_2 conduction band. Provided that the alkane layer is sufficiently thin, electrons can directly tunnel from carbon to the TiO_2 conduction band. Therefore, the electron injection barrier at the carbon/TiO_2 interface is effectively reduced by this energy-level alignment, resulting in an increased current when carbon is biased negative. The modulation of injection barriers by a low-κ molecular layer should be generally applicable to a variety of materials used in micro- and nanoelectronic fabrication.

KEYWORDS: molecular electronics • injection barrier • titanium dioxide • work function • monolayer • tunneling • electron transport

INTRODUCTION

Interfacial energetics play a central role in the physics of various micro- and nanoelectronic devices, including organic light-emitting diodes (OLEDs), polymer light-emitting diodes (PLEDs), organic field-effect transistors (OFETs), organic solar cells, and molecular electronic junctions (1−3). In many cases, the performance or characteristics of such electronic devices are greatly affected or controlled by interfacial charge injection barriers (4−18) at the interface between the contact electrode and the active layer. The problem is illustrated in Figure 1, for the case of a metal/TiO_2/metal junction, but similar issues apply to injection into molecular layers with highest occupied (HOMO) and lowest unoccupied (LUMO) molecular orbitals. Figure 1A shows that a hole injection barrier (Φ_h) can be defined as

$$\Phi_h = E_f - E_{HOMO} \quad (1)$$

where E_{HOMO} can be replaced by E_{VB} for a semiconductor. Likewise, the electron injection barrier (Φ_e) is defined as

$$\Phi_e = E_{LUMO} - E_f \quad (2)$$

where E_{LUMO} can be replaced by E_{CB} for a semiconductor.

In the example shown in Figure 1B, the electron injection barrier, Φ_e, prevents electron injection into the conduction band (CB) until the applied bias is large enough to overcome the barrier by field emission, thermionic emission, or tunneling. Both the electron and hole injection barriers can play dominant roles in charge transport in organic and molecular electronic devices and may ultimately determine the performance of OLEDs, PLEDs, and OFETs.

Several techniques have been employed to modulate the charge injection barrier in micro- and nanoelectronic devices through interface engineering, either by physical/chemical treatment of the contact electrode surface by mechanical polishing (19), oxygen plasma treatment (5, 20), and chemical treatment with acids and bases (21), etc., or by deposition of an additional "intermediate layer" between the contact electrode and the active layer (4, 10−12, 22−38). Although these interface engineering techniques have improved interfacial charge injection and enhanced the device

* Corresponding author. Tel.: 780-641-1760. E-mail: richard.mccreery@ualberta.ca.

Received for review October 15, 2008 and accepted December 29, 2008

† The Ohio State University.

‡ National Research Council of Canada.

§ University of Alberta.

DOI: 10.1021/am800126v

performance, a variety of mechanisms have been proposed to explain the effects, such as changes to metal work functions by surface dipoles (22−29), alteration of the chemical composition of the electrode surface (5, 20, 21), formation of a charge-transfer complex at the interface (10), band bending (4, 30), mobile ions (39), formation of a "built-in" electric field (11, 31), or enhancement of electron tunneling (12, 32−38). The electron-tunneling mechanism is particularly relevant to the current work, as will be discussed in more detail later.

Among various schemes of modulating the charge injection barrier, modification of the apparent metal work function (Φ_M) by deposition of a layer of polar molecules onto the contact metal surface has been examined in some detail (16, 22, 23, 26, 28, 29). Because Φ_M is defined by

$$\Phi_M = E_{vac} - E_f \quad (3)$$

where E_{vac} is the vacuum energy level, the effect of surface dipoles is often considered to result from a shift in E_{vac}. Although surface dipoles have been shown to result in improved electron injection and work function changes in the several cases cited above, the mechanism underlying the effect is not completely clear (40).

TiO_2 has been investigated as a component in memory devices based on metal/TiO_2/metal structures (41−44) and in carbon/molecule/TiO_2/metal heterojunctions (45−47). In both cases, injection of electrons from a metallic contact into the CB of TiO_2 partially or wholly controls the conductance of the device, as well as the memory effect in molecular heterojunctions (45). In the current report, we investigated the effects of several nonpolar and dipolar molecular layers on electron injection from a graphitic carbon contact into the TiO_2 CB. An unexpected enhancement of electron injection was observed upon the addition of a molecular layer between the carbon and TiO_2, which significantly affected the symmetry of the current/voltage behavior of the heterojunction. The current report focuses on the mechanism of the enhancement, in the context of "interface engineering". The effects of variation of the composition, thickness, polarity, and dielectric constant of the molecular layer on the current/voltage behavior of carbon/molecule/TiO_2/gold heterojunctions provided insights into the mechanism of enhanced electron injection.

EXPERIMENTAL SECTION

PPF Surface Derivatization. Pyrolyzed photoresist films (PPFs) were prepared as described previously (48, 49). Briefly, a positive photoresist AZ4330-RS (AZ Electronic Materials) was spun onto a 1.5 cm × 2 cm SiO_2/Si substrate at 6000 rpm for 40 s, followed by soft baking at 90 °C for 20 min. Next, a pattern of four strips (each strip is 0.5 mm wide) was made lithographically using a photomask. After patterning, substrates were pyrolyzed in a tube furnace by ramping the temperature to 1000 °C and holding for 1 h in a constant ~100 sccm stream of a forming gas containing 5% H_2 and 95% N_2. After cooling to room temperature, the samples were removed, cleaned, and modified.

PPF is structurally similar to glassy carbon and has a <0.5 nm surface roughness [root-mean-square value from atomic force microscopy (AFM) measurements], and a resistivity of 0.006 Ω · cm (48, 49). A BASi Epsilon-EC potentiostat (Bioanalytical Systems) is used to derivatize PPF substrates, with a conventional three-electrode configuration with PPF as the working electrode, Ag/Ag^+ as the reference electrode, and a coiled Pt wire as the auxiliary electrode. Derivatizaton of PPF was carried out using 1 mM concentrations of the corresponding diazonium salts, with 0.1 M *n*-tetrabutylammonium tetrafluoroborate ($TBABF_4$) as the supporting electrolyte in acetonitrile (ACN). Biphenyl (BP) and trifluoromethylphenyl (TFMP) films on PPF were prepared by sweeping the electrode from +0.4 to −0.4 V at 200 mV · s^{-1}. The derivatization of PPF with 1-aminooctane (C8N) was performed by amine oxidation (50, 51). The concentration of C8N was 5 mM in 0.1 M $TBABF_4$ in ACN, and controlled potential electrolysis (CPE) was applied at +0.8, +1.0, or +1.2 V for 10 min to obtain different thicknesses (0.98 ± 0.23, 1.59 ± 0.15, and 2.49 ± 0.13 nm, respectively). Initial and final scans were swept from 0 to +0.8, +1.0, or +1.2 V, respectively, before and after CPE to check for passivation of the PPF surface. The structures and calculated dipoles of the three molecular layers are shown in Figure S1 in the Supporting Information. Both diazonium reduction and amine oxidation are radical processes capable of forming multilayers, hence the need for thickness verification with AFM, as described previously (52).

Metal Surface Derivatization. Gold, silver, and copper substrates for Kelvin probe measurements were prepared by evaporating 10 nm of chromium on SiO_2/silicon as an adhesion layer, followed by evaporation of a 30 nm of metal on the chromium layer. The same derivatization conditions were used to modify gold surfaces with BP and TFMP molecules as those to modify PPF surfaces. Copper and silver surfaces were modified by dipping copper or silver substrates in a 1 mM BP or TFMP diazonium salt solution in ACN for 5 s.

Junction Fabrication and Characterization. Junctions were fabricated using a "crossed junction" design described previously (53−56). Briefly, derivatized PPF substrates were placed in a PVD-75 electron beam evaporator (Kurt J. Lesker), then a metal oxide layer and a top gold contact were deposited through a shadow mask with 0.5 mm strips oriented perpendicular to the PPF strips, resulting in a 0.5 mm × 0.5 mm junction (geometric area = 0.0025 cm^2). The deposition rate and film thickness were monitored using a quartz crystal microbalance. The O_2 and H_2O partial pressures in the evaporation chamber were monitored using a residual gas analyzer (RGA/200, Stanford Research Systems). Metal oxides including TiO_2, Al_2O_3, and SiO_2 were deposited at 0.01−0.02 nm · s^{-1} with ~1.5×10^{-5} Torr of O_2 and $(2-8) \times 10^{-6}$ Torr of H_2O. The top gold contact was deposited at ~0.02 nm · s^{-1}. Junction notation follows a layer format, beginning at the bottom and listing the thickness of the molecular layer, oxide layer, and top contact in parentheses (nanometer units). Thus, PPF/C8N(1)/TiO_2(10)/Au(15) designates a junction with a 1 nm octylamine layer on PPF, a 10 nm TiO_2 layer, and 15 nm gold layer as the top contact. Electronic testing of junctions was performed in air as discussed previously (54, 56) but with a "four-wire" configuration in this work. The bias (PPF relative to gold) was applied between the PPF and gold strips through tungsten probes mounted on 3-axis micromanipulators. A "four-wire" configuration was used to compensate for ohmic losses in the PPF and gold strips. A schematic diagram of a test structure and a micrograph of an actual device with the "four-wire" arrangement are shown in Figure 2. All current density (J, A · cm^{-2}) vs voltage (V) curves are obtained at a scan rate of 1000 V · s^{-1}.

Work Function Measurements by the Kelvin Probe Technique. The work functions of PPF samples and metal substrates were measured using a scanning Kelvin probe instrument (SKP5050, KP Technology) in the laboratory ambient. In the Kelvin probe technique, the conductive substrate and a Au tip (diameter = 2 mm) form a capacitor. The Au tip is oscillated by a voice coil driver, inducing an alternating current. This

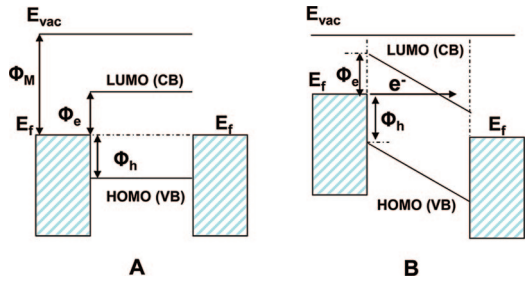

FIGURE 1. Schematic representation of the energy levels at metal/organic or metal/semiconductor interfaces. (A) Situation for an organic layer or a semiconductor on a conductive surface where there is no interfacial dipole at zero bias. (B) Same as part A but with a bias. Abbreviations: E_f, metal Fermi level; E_{vac}, vacuum level; CB, conduction band; VB, valence band; Φ_M, metal work function.

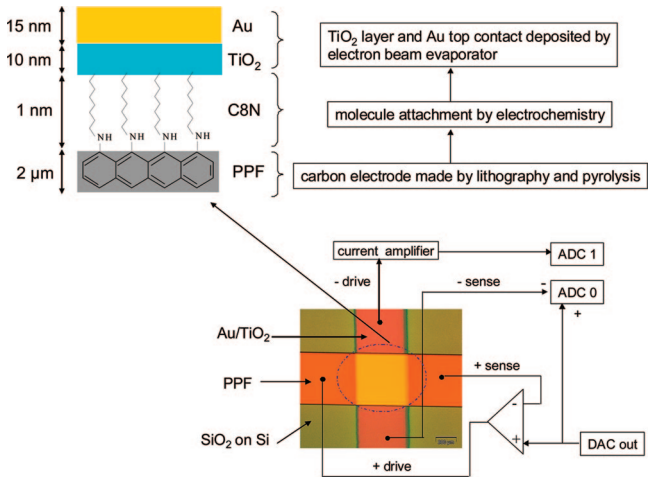

FIGURE 2. Schematics of the junction structure, instrumentation for electrical measurement, and brief fabrication procedures. The upper left drawing is a schematic cross-sectional view of a junction, with layer thicknesses (not drawn to scale). In some cases as noted in the text, either the alkane layer (C8N), the TiO_2 layer, or both is replaced with SiO_2, Al_2O_3, or other molecules. The lower drawing is a micrograph of an actual junction with a "four-wire" arrangement, which corrects for ohmic loss in the contact leads of the "crossed junction" geometry. DAC applies the bias, and ADC0 monitors the *iR*-corrected voltage across the junction.

current is nulled when the applied direct current bias equals the contact potential difference (CPD) between the substrate and the Au tip. So, the CPD is a direct measure of the work function of the substrate relative to that of the Au tip. The Au tip work function was determined daily by referencing to a freshly cleaved highly ordered pyrolytic graphite (HOPG) surface, which is known to have a reproducible work function of 4.475 eV in air (57).

Calculations. Molecular dipole moments on PPF were calculated with *Gaussian '03*. Because all three molecules C8N, BP, and TFMP are covalently bonded to the graphitic PPF surface, calculations of the overall molecular dipole moments were performed on a series of molecular species designed to model this interface. A phenyl moiety was bonded through a covalent linkage to each molecular component to resemble the PPF substrate. Energy minimization was realized with an STO-3G basis set at the Hartree–Fock level, while the dipole moment was calculated using the more comprehensive HF/6-31G basis set (58, 59). Energy levels and energy gaps for C8N, BP, and TFMP were calculated by *Gaussian '03*, using the DFT/B3LYP method with a 6-31G(d) basis set.

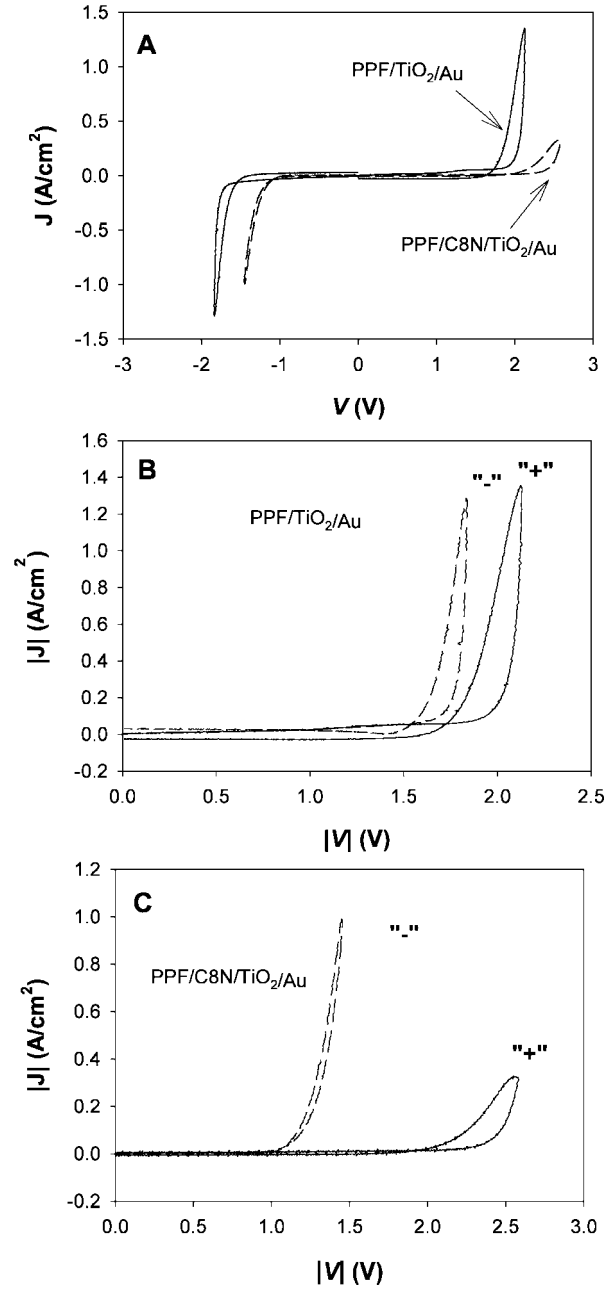

FIGURE 3. (A) $J-V$ curves (1000 V · s^{-1}) for PPF/TiO_2(10)/Au junctions (solid curve) and PPF/C8N(1)/TiO_2(10)/Au junctions (dashed curve), with and without a 1 nm insertion layer of C8N between PPF and TiO_2. (B) $|J|-|V|$ curve for PPF/TiO_2(10)/Au. (C) $|J|-|V|$ curve for PPF/C8N(1)/TiO_2(10)/Au. "+" denotes positive bias, and "−" denotes negative bias.

RESULTS

Figure 3A shows an overlay of current density (J) vs voltage (V) curves for PPF/TiO_2(10)/Au and PPF/C8N(1)/TiO_2(10)/Au junctions [i.e., with and without an alkane (C8N) layer]. PPF/TiO_2/Au junctions show a nearly symmetric $J-V$ curve. The hysteresis observed with TiO_2 has been discussed elsewhere (45, 46) and is not the subject of the current report. Asymmetry between the current observed at negative bias and that at positive bias was evaluated by comparing the voltages required to obtain the same magnitude of J. For PPF/TiO_2/Au (Figure 3A), biases of +1.94 and −1.69 V are required to reach $|J| = 0.1$ A · cm^{-2}. The difference

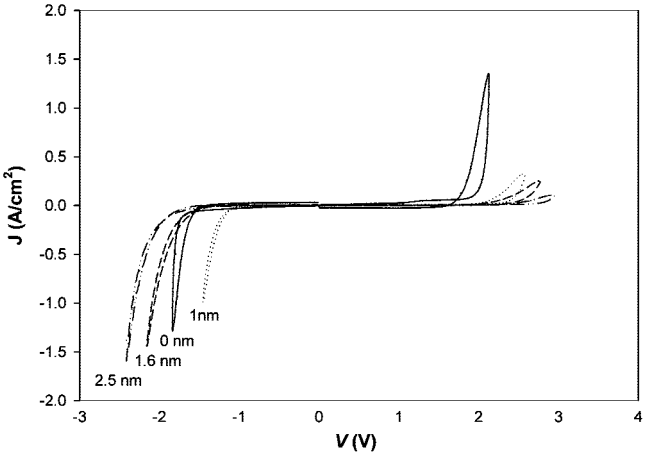

FIGURE 4. $J-V$ curves for PPF/C8N/TiO_2(10)/Au junctions where the thickness of the C8N varies: no C8N layer (solid curve), 1 nm (dotted curve), 1.6 nm (dashed curve), and 2.5 nm (dot-dashed curve).

between the absolute values of these voltages is 0.25 V and can be defined as the voltage asymmetry, ΔV. Surprisingly, when an alkane layer is deposited between PPF and TiO_2, the junctions become more conductive for negative bias. We refer to this counterintuitive effect as "anomalous" because the addition of a nominally insulating alkane layer significantly *increases* the current magnitude for negative bias. The value of ΔV at $|J| = 0.1$ A $\cdot$ cm^{-2} for the PPF/C8N(1)/TiO_2(10)/Au junction is 1.27 V, corresponding to a change of $\sim$1 V to the voltage asymmetry from the addition of the alkane layer. To better illustrate the increased asymmetry, $|J|-|V|$ curves for each case are also shown in parts B and C of Figure 3, respectively.

The pronounced effect of the thickness of the molecular layer on the $J-V$ behavior is shown in Figure 4, for PPF/C8N/TiO_2(10)/Au junctions with C8N thicknesses of 0.98 ± 0.23, 1.59 ± 0.15, and 2.49 ± 0.13 nm, as determined by an AFM scratching technique (52). As the thickness of the alkane layer increases, each $J-V$ curve shifts toward more negative voltage at negative bias and toward more positive voltage at positive bias, meaning that the junctions become less conductive. In fact, for C8N layers with thickness greater than 1.6 nm, the junctions are less conductive than control junctions (PPF/TiO_2/Au) at both negative bias and positive bias, and no anomalous effect is observed.

To explore the role of identity of the inserted layer on the observed anomalous effect, the C8N layer was replaced by inorganic films. Electron beam evaporation was used to deposit thin layers (1 nm by mass) of SiO_2 or Al_2O_3 onto bare PPF substrates immediately before TiO_2 deposition. An overlay of $J-V$ curves for PPF/SiO_2(1)/TiO_2(10)/Au and PPF/TiO_2(10)/Au is shown in Figure 5A. From the analysis of these curves, it is apparent that a 1 nm layer of SiO_2 has the same effect on the symmetry of the response that was observed for C8N, with an overlay of the response for the SiO_2 and C8N devices showing nearly identical $J-V$ behavior (Figure 5B). However, as shown in Figure 5C, when C8N is replaced with Al_2O_3, the response is markedly different at negative bias. That is, the current is decreased for both polarities, and the inserted Al_2O_3 does not "assist" electron injection at negative bias, as was observed with C8N and SiO_2. Finally, $J-V$ curves of PPF/SiO_2/TiO_2(10)/Au junctions with increasing SiO_2 thicknesses are shown in Figure 5D. As the thickness of SiO_2 increases, the current decreases at both negative and positive bias, similar to but more pronounced than the effect observed with the C8N layers (Figure 4).

When TiO_2 was replaced with e-beamed SiO_2 or Al_2O_3, the observed currents were greatly reduced, as shown in Figure 6A,B. The insulating materials suppress the current by a factor of >100 compared to TiO_2. Figure 6C shows overlays of $J-V$ curves for PPF/C8N(1)/SiO_2(10)/Au and PPF/SiO_2(10)/Au, and Figure 6D shows a corresponding series of curves for Al_2O_3. In both cases, the C8N layer only causes a slight increase in the resistance, and no "anomalous" response is observed, as was the case for junctions containing TiO_2. In a summary of the results to this point, the thicknesses and identities of both the molecular and oxide layers have strong effects on the $J-V$ responses of the various heterojunctions. We now consider the effect of surface dipoles in the molecular layer.

As noted in the Introduction, surface dipoles can modify the effective work functions of metal surfaces (26, 28, 60, 61), so molecules with different molecular dipoles were covalently attached to PPF before TiO_2 deposition. BP, C8N, and TFMP were compared, as molecules with minimal dipole (BP) or oriented toward (C8N, -1.82 D) or away (TFMP, $+4.77$ D) from the PPF surface, as shown by Figure S1 in the Supporting Information. Table 1 shows the pronounced effect of the surface dipole on the work function observed with a Kelvin probe in air, and a more extensive table is provided in the Supporting Information. The BP modification results in a small (-0.02 V) shift in the apparent work function of PPF, while C8N causes a 0.21 V decrease and TFMP a 0.51 V increase in the work function. Figure 7 shows the effect visually, for a scanning Kelvin probe image of a single PPF strip modified at one end with C8N and the other with TFMP. As indicated in both the table and Figure 7, the molecular surface modification resulted in observed work functions ranging over $\sim$0.7 V.

Figure 8 shows overlays of $J-V$ curves for PPF/molecule/TiO_2(10)/Au junctions with various molecular dipoles, as well as PPF/TiO_2(10)/Au alone. In this series of junctions, the molecular layer identity varies but layer thicknesses are similar for all junction components. Figure 8 shows that all three junctions containing a thin ($\sim$1 nm) molecular layer show enhanced current compared to the junction with no molecular layer for negative bias. Thus, an anomalous increase in the current is observed with a variety of materials that have a range of dipole moment magnitudes and orientations, establishing that the molecular dipole and possible work function change do not explain the anomalous effect and another mechanism must be responsible.

DISCUSSION

The anomalous effect that an increased current results from an insulating molecular layer is observed when a $\sim$1-nm-thick layer of either organic molecules (C8N, BP, and TFMP) or an inorganic material (SiO_2) is deposited between

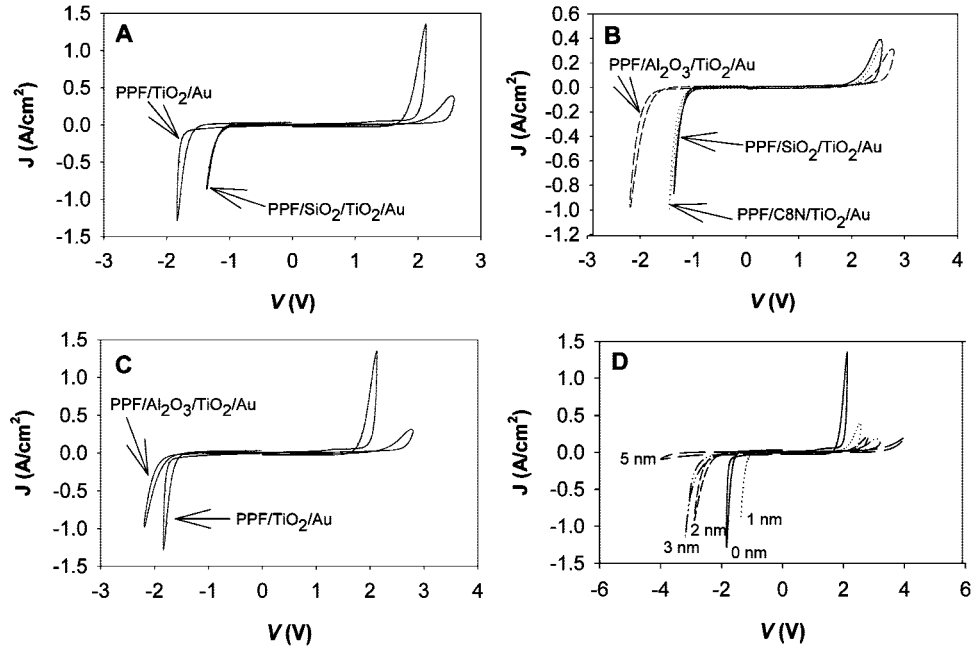

FIGURE 5. (A) $J-V$ curves for PPF/TiO_2(10)/Au and PPF/SiO_2(1)/TiO_2(10)/Au junctions. (B) $J-V$ curves for PPF/C8N(1)/TiO_2(10)/Au, PPF/SiO_2(1)/TiO_2(10)/Au, and PPF/Al_2O_3(1)/TiO_2(10)/Au junctions. (C) $J-V$ curves for PPF/TiO_2(10)/Au and PPF/Al_2O_3(1)/TiO_2(10)/Au junctions. (D) $J-V$ curves for PPF/SiO_2/TiO_2(10)/Au junctions where the SiO_2 thickness varies from 0 to 5 nm.

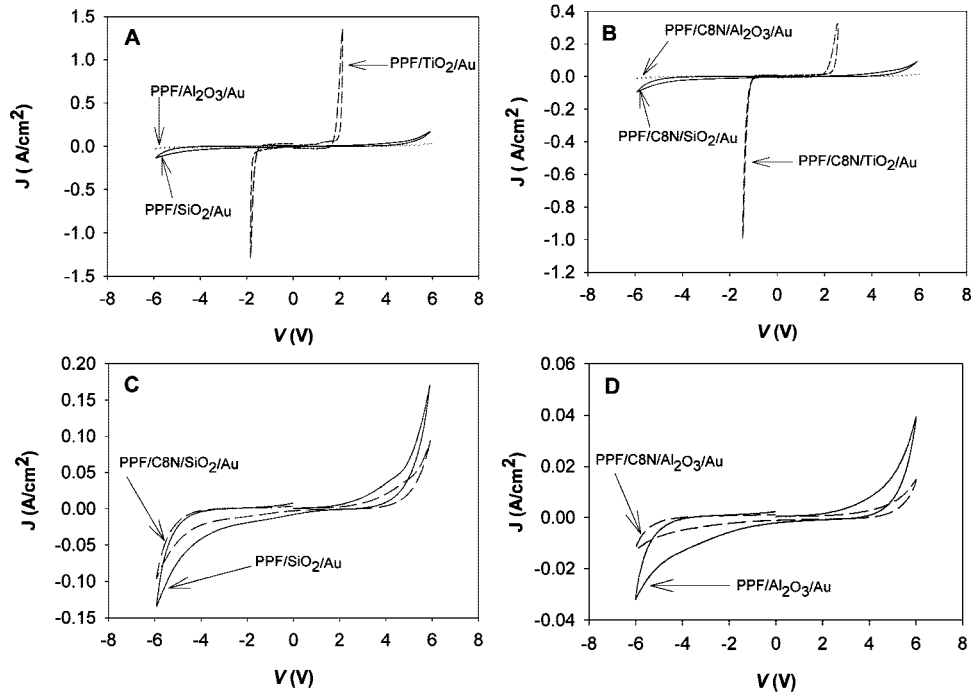

FIGURE 6. (A) $J-V$ curves for PPF/SiO_2(10)/Au, PPF/Al_2O_3(10)/Au, and PPF/TiO_2(10)/Au junctions. (B) $J-V$ curves for PPF/C8N(1)/SiO_2(10)/Au, PPF/C8N/Al_2O_3(10)/Au, and PPF/C8N/TiO_2(10)/Au junctions. (C) $J-V$ curves for PPF/SiO_2(10)/Au junctions, with and without a 1 nm insertion layer of C8N between PPF and SiO_2. (D) $J-V$ curves for PPF/Al_2O_3(10)/Au junctions, with and without a 1 nm insertion layer of C8N between PPF and Al_2O_3.

PPF and TiO_2 in a PPF/TiO_2/Au junction but is not observed with Al_2O_3 (for convenience of discussion, the deposited layer between PPF and TiO_2 will be named "the intermediate layer" in the following text). The effect is also strongly dependent on the thickness of the intermediate layer, with no current enhancement observed for thicknesses of 1.6 nm or greater. The fact that the effect is independent of the orientation or magnitude of the molecular dipole moment excludes the possibility that the electron injection barrier is reduced through a change in the apparent work function of PPF. Moreover, to the authors' knowledge, there are no known charge-transfer states between PPF and C8N, BP, TFMP, or SiO_2. Thus, a model that explains the anomalous effect must take into account the properties of the different layers that lead to particular junction behavior. On the other hand, a similarity between an alkane (C8N) and e-beamed SiO_2 is their low dielectric constant, in the range of 2–4 (31, 62–66), while Al_2O_3 has a relatively high dielectric

Table 1. Work Functions (WFs) Measured by a Kelvin Probe in Air

sample	WF vs Au[a] (eV)	absolute WF[b] (eV)	WF shift[c] (eV)
PPF	0.212 ± 0.010	4.932 ± 0.012	
PPF/C8N	0.006 ± 0.011	4.726 ± 0.013	−0.206 ± 0.015
PPF/TFMP	0.723 ± 0.011	5.443 ± 0.013	0.511 ± 0.015
PPF/BP	0.192 ± 0.012	4.912 ± 0.014	−0.020 ± 0.015
PPF/TiO_2	0.089 ± 0.003	4.684 ± 0.007	
PPF/C8N/TiO_2	0.095 ± 0.003	4.678 ± 0.007	0.006 ± 0.004
PPF/TFMP/TiO_2	0.069 ± 0.007	4.704 ± 0.009	−0.020 ± 0.008
PPF/BP/TiO_2	0.011 ± 0.008	4.762 ± 0.007	−0.078 ± 0.009
Au	0.051 ± 0.007	4.820 ± 0.012	
Au/TiO_2	0.037 ± 0.006	4.802 ± 0.10	−0.014 ± 0.009

[a] Mean ± standard deviation, relative to the Au tip of the Kelvin probe instrument. [b] An absolute work function was obtained by referencing to a freshly cleaved HOPG surface (4.475 eV). [c] The work function shift is the change in the observed WF caused by the addition of a molecular layer (BP, C8N, or TFMP). For example, the work function shift for PPF/C8N is calculated relative to PPF, while PPF/C8N/TiO_2 is relative to PPF/TiO_2.

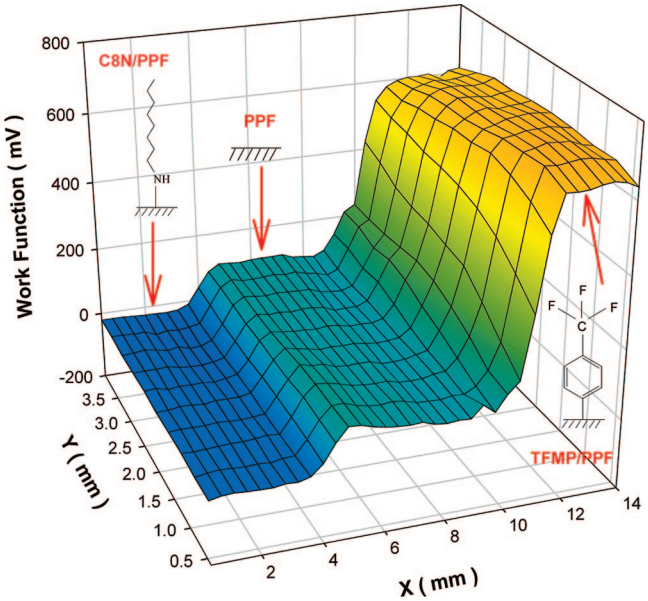

FIGURE 7. Scanning Kelvin probe image of a modified PPF sample. One end (X < 5 mm) of the PPF sample was modified by C8N molecules, the other end (X > 12 mm) was modified by TFMP molecules, and the middle part is bare PPF. The scanning size is ~14 mm × 4 mm. The work function values at the Y axis are referenced to the Au tip of the scanning Kelvin probe instrument.

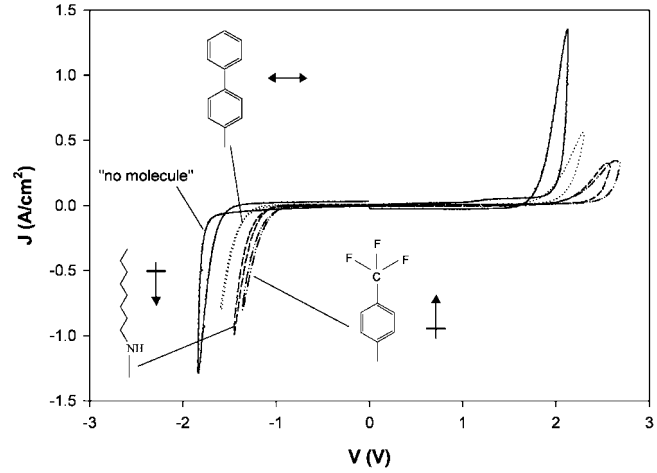

FIGURE 8. Comparison of $J-V$ curves for PPF/TiO_2(10)/Au junctions, with and without three structurally different molecular insertion layers. Each molecule has a different dipole moment whose direction is defined in the text and is denoted by the arrows in the figure.

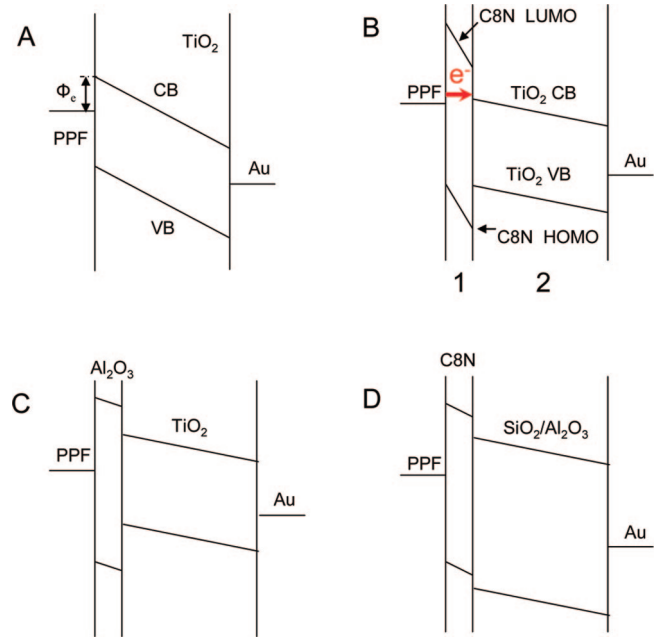

FIGURE 9. Schematic energy level diagrams that show the mechanisms that underlie various devices discussed in the text: (A) PPF/TiO_2(10)/Au; (B) PPF/C8N(1)/TiO_2(10)/Au; (C) PPF/Al_2O_3(1)/TiO_2(10)/Au; (D) PPF/C8N(1)/SiO_2(10) or Al_2O_3(10)/Au.

constant, in the range of 7−11 (67−70). On the basis of the experimental observations, we propose herein a mechanism of electron injection barrier reduction via energy level alignment at the PPF/TiO_2 (metal/semiconductor) interface, with a low-κ dielectric film as a tunneling barrier, which permits energy level alignment.

Figure 9 shows schematic energy level diagrams that illustrate a possible mechanism for the enhanced current observed at low bias. In all cases shown, PPF is negatively biased such that electrons are injected from the PPF, through any intermediate layers into the TiO_2 CB. Because of the low valence band (VB) energy of TiO_2 (~−7 eV relative to a vacuum), hole transport is unlikely in TiO_2 heterojunctions. For PPF/TiO_2/Au junctions without the intermediate layer (Figure 9A), the electron injection barrier (Φ_e) at the PPF/TiO_2 interface is given by eq 2, i.e., the energy difference between the PPF Fermi level (E_f) and the TiO_2 CB (E_{CB}). Taking the TiO_2 CB energy as −3.95 V (71), the measured PPF work function yields $\Phi_e = 1.0$ eV. Similarly, the electron injection barrier at the Au/TiO_2 interface is approximately 0.87 eV. These injection barriers predict asymmetry opposite to that observed in Figure 3A for the PPF/TiO_2/Au junction, in that the lower injection barrier at Au should cause higher current for positive bias. However, comparison of the work functions of PPF and Au after TiO_2 modification results in electron injection barrier at a PPF smaller than that at Au (0.73 vs 0.85 eV), consistent with the modest observed asymmetry.

An energy diagram for the situation where a thin, low-κ dielectric film is used as an insertion layer is shown in Figure 9B. A simple model to describe the voltage drop across the molecular and TiO_2 layers assumes that they behave like two capacitors in series, which yields eqs 4 and 5:

$$V_1 = \frac{(\kappa_2/d_2)V_b}{\kappa_1/d_1 + \kappa_2/d_2} \quad (4)$$

$$V_2 = \frac{(\kappa_1/d_1)V_b}{\kappa_1/d_1 + \kappa_2/d_2} \quad (5)$$

where V_b is the applied bias, V_i is the voltage drop across the ith layer, κ_i is the dielectric constant, and d_i is the thickness of the ith layer, respectively (32). Note that the voltage drop is generally larger across the layer with the lower dielectric constant. For example, with $d_1 = 1$ nm, $d_2 = 10$ nm, and $\kappa_2 = 50$, V_1 for $\kappa_1 = 2.5$ is $0.67V_b$, while that for $\kappa_1 = 10$ is $0.33V_b$.

The dielectric constant of TiO_2 varies significantly with the microstructure and composition, with typically reported values in the range of 50−110 and values as low as 15 reported for e-beam-deposited TiO_2 (72). When materials with low dielectric constants (for example, alkanes or SiO_2) are deposited between PPF and TiO_2, the applied bias is dropped mostly across the low-κ layer, as shown in Figure 9B. The smaller voltage drop across the relatively high-κ TiO_2 results in a small shift in the CB energy, and the PPF Fermi level may shift relative to the CB energy, thus reducing the injection barrier. Once the PPF Fermi level and the CB energy are aligned for sufficiently negative bias, tunneling can occur through the thin intermediate layer from the PPF into the TiO_2 CB. The electron injection barrier at the PPF/TiO_2 interface is effectively reduced, resulting in an increase in the current for negative bias shown in Figure 3. If the low-κ layer is too thick, however, the tunneling rate is too slow even with alignment of the energy levels, thus defeating the enhanced current (Figure 4). When a relatively high-κ material is used, i.e., Al_2O_3 instead of C8N or SiO_2, less voltage is dropped across the Al_2O_3 film and the energy levels of the PPF and the TiO_2 CB are not well aligned. As shown in Figure 9C, the electron injection barrier at the PPF/TiO_2 interface is larger than that in the situation where no Al_2O_3 is present. When SiO_2 or Al_2O_3 are substituted for TiO_2, their higher CB energy prevents electron injection over the range of voltage examined (Figure 9D).

To further generalize the dependence of the energy level alignment on the dielectric constant and thickness of the intermediate layer, calculations based on eqs 4 and 5 were used to simulate the dependence of the electron injection barrier on the dielectric constant ratio and the thickness of the intermediate layer. Φ_e was assumed to be 0.98 eV at zero bias, and a bias of −1.35 V was used for the examples shown in Figure 10. Figure 10A shows the dependence of Φ_e on the dielectric constant ratio between TiO_2 and the intermediate layer, for several thickness ratios. For a thickness ratio of 10 used in the devices of Figures 3 and 5, the injection barrier decreases to zero for a dielectric constant ratio of ∼25. For the case of PPF/C8N/TiO_2/Au junctions, with a

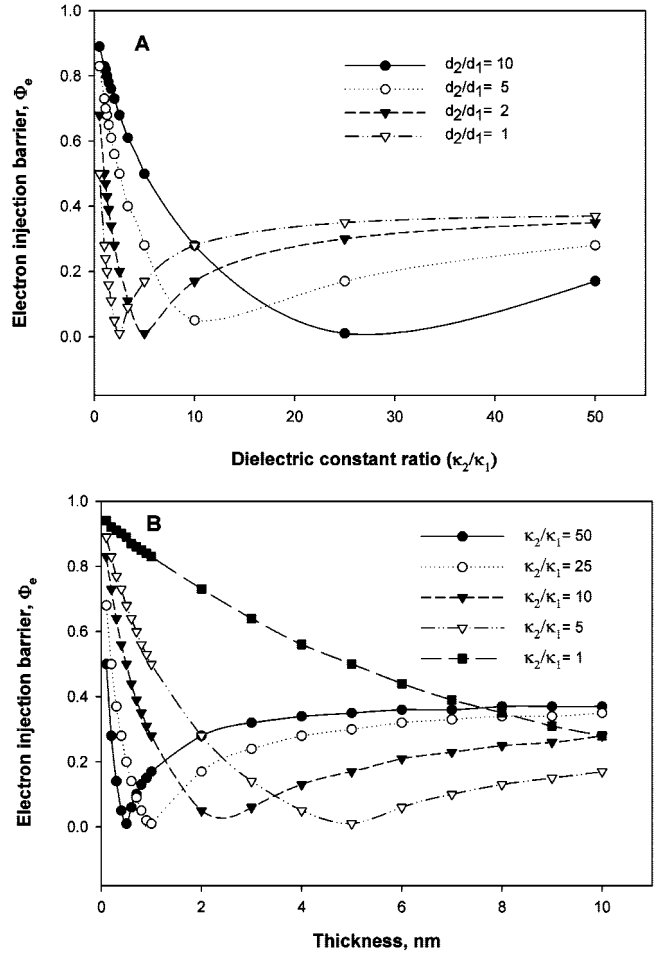

FIGURE 10. (A) Dependence of the electron energy barrier between the PPF Fermi level and the TiO_2 CB on the dielectric constant ratio of the TiO_2 layer and the intermediate layer. The four curves represent various thickness ratios of the two layers. (B) Calculated dependence of the injection barrier on the thickness of the intermediate layer. The five curves represent various dielectric constant ratios. κ_1, κ_2, and d_1, d_2 are the dielectric constants and thicknesses of the intermediate layer and the TiO_2 layer, respectively. In the calculations, $\kappa_2 = 50$ and $d_2 = 10$ nm for TiO_2 are constant and under a bias of −1.35 V.

dielectric constant ratio of ∼20, a bias of −1.35 V is sufficient to inject electrons into TiO_2, as observed experimentally (Figure 3A). However, when C8N is replaced with Al_2O_3 to produce a dielectric ratio of ∼5, Φ_e is nonzero (∼0.5 eV), and the anomalous current is absent, as shown in Figure 5C. The dependence of calculated Φ_e on the thickness of the intermediate layer is shown in Figure 10B, demonstrating an optimum thickness of the intermediate layer to achieve a minimum Φ_e. For a dielectric constant ratio ∼25 for the case of PPF/C8N/TiO_2/Au junctions, the optimum thickness of the C8N is shown to be ∼1 nm, which is consistent with the experimental result in Figure 4. As the ratio of dielectric constants decreases, Φ_e is minimized for thicker intermediate layers, also shown in Figure 10B. However, because tunneling decreases exponentially with distance, intermediate layers much thicker than 1 nm significantly reduce the anomalous effect, as shown experimentally in Figure 4.

Energy levels of the intermediate layer may not be critical to the anomalous tunneling, as long as the HOMO (VB) or

Table 2. Calculated Energy Levels and Energy Gaps for C8N, BP, TFMP, and TiO_2

material	HOMO or VB (eV)	LUMO or CB (eV)	energy gap (eV)
C8N[a]	−6.21	1.99	8.20
TFMP[a]	−7.24	−0.72	6.52
BP[a]	−6.04	−0.68	5.36
TiO_2[b]	−6.95	−3.95	3.00
SiO_2[c]	−10.2	−1.3	8.9
Al_2O_3[c]	−9.5	−2.5	7.0

[a] Values calculated by *Gaussian '03*, using the DFT/B3LYP method with a 6-31G(d) basis set. [b] Literature values from ref 71. [c] Literature values from ref 76.

the LUMO (CB) does not align with the PPF Fermi level (in this case, a different mechanism will take over) so that the intermediate layer only acts as a tunneling barrier. Table 2 lists the calculated and literature values of energy levels and energy gaps for the materials used in this work. According to the Kelvin probe data in Table 1, the PPF work function is ∼4.93 eV. The PPF Fermi level falls below the TiO_2 CB of ∼1 eV, which provides a good chance for energy level alignment. However, when TiO_2 is replaced with high-band-gap materials like SiO_2 or Al_2O_3 (Figure 6), the large energy difference between the PPF Fermi level and the SiO_2/Al_2O_3 CB prevents energy level alignment of the PPF Fermi level with the oxide CB, as illustrated in Figure 9D, and no anomalous tunneling effect is observed.

As is apparent from the above discussions, the thickness and dielectric constant of the intermediate layer play important roles in aligning energy levels and reducing Φ_e. However, the absence of an effect of the molecular dipole (Figure 8) was unexpected. Although a dipolar molecular layer can significantly change the injection efficiency and work functions in other devices (22−29) as well as the apparent PPF work function (Table 1), changes in the molecular dipole did not significantly affect the injection observed in Figure 8. Furthermore, the addition of TiO_2 on top of the molecule effectively cancels the observed change in the work function. In a recent publication, Demirkan et al. (40) reported similar results for organic heterojunctions: polar self-assembled monolayers (SAMs) can change the apparent work function of a gold substrate, but the energy level alignment between gold and an organic semiconductor is not necessarily changed. The authors attributed the unchanged work function to the suppression of molecular dipoles by deposition of the organic semiconductor, cancelling the energy level alignment between the metal and the semiconductor. Although the mechanism of "cancellation" of the molecular dipole by TiO_2 is not clear, the outcome itself can explain why the molecular dipoles do not contribute to the anomalous tunneling effect reported here.

Energy level alignment at metal/organic interfaces has been studied extensively in organic electronics but for much thicker molecular layers than studied here. Previous studies have shown that desirable characteristics of molecular electronic devices, e.g., resonant tunneling or negative differential resistance (73−75), etc., can be achieved via energy level alignment at the metal/molecule interface. In turn, we showed in this paper that energy level alignment at the metal/semiconductor interface can be achieved by utilizing the distinctive dielectric properties of the two materials in the PPF/alkane/TiO_2/Au hybrid molecular junctions. The consequences of the current work should have important implications to the understanding of interface energetics and rational design of molecular or organic electronic devices to achieve desirable functions. However, the intermediate layer must be a very thin and low-κ material to allow tunneling, and such layers are rare in organic electronics. Nevertheless, the modulation of injection barriers with a thin and a low-κ molecular layer should be generally applicable to a variety of materials used in micro- and nanoelectronic fabrication.

CONCLUSIONS

We demonstrate in this paper that the electron injection barrier at the PPF/TiO_2 (metal/semiconductor) interface can be reduced via interface engineering. An ultrathin layer of organic molecules or inorganic materials with low dielectric constant was deposited between the carbon electrode and TiO_2 as an insertion layer. Because of its low-κ dielectric property, a large fraction of the applied bias appears across the inserted film, resulting in an energy level alignment between the PPF Fermi level and the TiO_2 CB. Electrons can tunnel directly from the PPF Fermi level to the TiO_2 CB, resulting in an enhanced current compared to devices containing only TiO_2. This effect can compensate for a moderate injection barrier, depending on the relative dielectric constants and thicknesses of the insertion layer and the oxide layer. In this work, a ∼1 eV electron injection barrier was compensated for. While the anomalous tunneling is demonstrated here for TiO_2 containing molecular heterojunctions, the findings should be generally applicable to various materials, including organic and inorganic materials used in micro- or nanoelectronic fabrication, which are sufficiently thin to permit tunneling.

Acknowledgment. This work was supported by the National Science Foundation through Project 0211693 from the NSF (U.S.) Analytical and Surface Chemistry Division, the University of Alberta, the National Research Council of Canada, and the Alberta Ingenuity Fund. The authors also acknowledge Dr. Adam J. Bergren for his useful suggestions and assistance with the manuscript.

Supporting Information Available: Structures and dipole moments of modified surfaces and a more extensive table of observed work functions. This material is available free of charge via the Internet at http://pubs.acs.org.

REFERENCES AND NOTES

(1) Ishii, H.; Sugiyama, K.; Ito, E.; Seki, K. *Adv. Mater.* **1999**, *11*, 605–625.
(2) Cahen, D.; Kahn, A. *Adv. Mater.* **2003**, *15*, 271–277.
(3) Heimel, G.; Romaner, L.; Zojer, E.; Bredas, J.-L. *Acc. Chem. Res.* **2008**, *41*, 721–729.
(4) Hung, L. S.; Tang, C. W.; Mason, M. G. *Appl. Phys. Lett.* **1997**, *70*, 152–154.
(5) Wu, C. C.; Wu, C. I.; Sturm, J. C.; Kahn, A. *Appl. Phys. Lett.* **1997**, *70*, 1348–1350.

(6) Deng, Z. B.; Ding, X. M.; Lee, S. T.; Gambling, W. A. *Appl. Phys. Lett.* **1999**, *74*, 2227–2229.
(7) Ganzorig, C.; Kwak, K.-J.; Yagi, K.; Fujihira, M. *Appl. Phys. Lett.* **2001**, *79*, 272–274.
(8) Koch, N.; Elschner, A.; Schwartz, J.; Kahn, A. *Appl. Phys. Lett.* **2003**, *82*, 2281–2283.
(9) Chen, B. J.; Sun, X. W.; Divayana, Y.; Tay, B. K. *J. Appl. Phys.* **2005**, *98*, 046107.
(10) Hanson, E. L.; Guo, J.; Koch, N.; Schwartz, J.; Bernasek, S. L. *J. Am. Chem. Soc.* **2005**, *127*, 10058–10062.
(11) Brown, T. M.; Friend, R. H.; Millard, I. S.; Lacey, D. J.; Burroughes, J. H.; Cacialli, F. *Appl. Phys. Lett.* **2000**, *77*, 3096–3098.
(12) Park, J. H.; Park, O. O.; Yu, J.-W.; Kim, J. K.; Kim, Y. C. *Appl. Phys. Lett.* **2004**, *84*, 1783–1785.
(13) Blanchet, G. B.; Fincher, C. R.; Lefenfeld, M.; Rogers, J. A. *Appl. Phys. Lett.* **2004**, *84*, 296–298.
(14) Chen, W.; Huang, C.; Gao, X. Y.; Wang, L.; Zhen, C. G.; Qi, D.; Chen, S.; Zhang, H. L.; Loh, K. P.; Chen, Z. K.; Wee, A. T. S. *J. Phys. Chem. B* **2006**, *110*, 26075–26080.
(15) McDowell, M.; Hill, I. G.; McDermott, J. E.; Bernasek, S. L.; Schwartz, J. *Appl. Phys. Lett.* **2006**, *88*, 073505.
(16) Khodabakhsh, S.; Sanderson, B. M.; Nelson, J.; Jones, T. S. *Adv. Funct. Mater.* **2006**, *16*, 95–100.
(17) Yokota, K.; Taniguchi, M.; Kawai, T. *J. Am. Chem. Soc.* **2007**, *129*, 5818–5819.
(18) Heimel, G.; Romaner, L.; Zojer, E.; Bredas, J. L. *Nano Lett.* **2007**, *7*, 932–940.
(19) Jung, S.; Park, N. G.; Kwak, M. Y.; Kim, B. O.; Choi, K. H.; Cho, Y. J.; Kim, Y. K.; Kim, Y. S. *Opt. Mater.* **2003**, *21*, 235–241.
(20) Choi, H. W.; Kim, S. Y.; Kim, K.-B.; Tak, Y.-H.; Lee, J.-L. *Appl. Phys. Lett.* **2005**, *86*, 012104.
(21) Nuesch, F.; Rothberg, L. J.; Forsythe, E. W.; Le, Q. T.; Gao, Y. *Appl. Phys. Lett.* **1999**, *74*, 880–882.
(22) Campbell, I. H.; Kress, J. D.; Martin, R. L.; Smith, D. L.; Barashkov, N. N.; Ferraris, J. P. *Appl. Phys. Lett.* **1997**, *71*, 3528–3530.
(23) Appleyard, S. F. J.; Day, S. R.; Pickford, R. D.; Willis, M. R. *J. Mater. Chem.* **2000**, *10*, 169–173.
(24) Crispin, X.; Geskin, V.; Crispin, A.; Cornil, J.; Lazzaroni, R.; Salaneck, W. R.; Bredas, J. L. *J. Am. Chem. Soc.* **2002**, *124*, 8131–8141.
(25) Koch, N.; Kahn, A.; Ghijsen, J.; Pireaux, J. J.; Schwartz, J.; Johnson, R. L.; Elschner, A. *Appl. Phys. Lett.* **2003**, *82*, 70–72.
(26) Boer, B. d.; Hadipour, A.; Mandoc, M. M.; Woudenbergh, T. v.; Blom, P. W. M. *Adv. Mater.* **2005**, *17*, 621–625.
(27) Braun, S.; Osikowicz, W.; Wang, Y.; Salaneck, W. R. *Org. Electron.* **2007**, *8*, 14–20.
(28) Cho, C.-P.; Tao, Y.-T. *Langmuir* **2007**, *23*, 7090–7095.
(29) Wu, K.-Y.; Tao, Y.-T.; Huang, H.-W. *Appl. Phys. Lett.* **2007**, *90*, 241104.
(30) Ihm, K.; Kang, T.-H.; Kim, K.-J.; Hwang, C.-C.; Park, Y.-J.; Lee, K.-B.; Kim, B.; Jeon, C.-H.; Park, C.-Y.; Kim, K.; Tak, Y.-H. *Appl. Phys. Lett.* **2003**, *83*, 2949–2951.
(31) Malinsky, J. E.; Veinot, J. G. C.; Jabbour, G. E.; Shaheen, S. E.; Anderson, J. D.; Lee, P.; Richter, A. G.; Burin, A. L.; Ratner, M. A.; Marks, T. J.; Armstrong, N. R.; Kippelen, B.; Dutta, P.; Peyghambarian, N. *Chem. Mater.* **2002**, *14*, 3054–3065.
(32) Kim, Y.-E.; Park, H.; Kim, J.-J. *Appl. Phys. Lett.* **1996**, *69*, 599–601.
(33) Jabbour, G. E.; Kawabe, Y.; Shaheen, S. E.; Wang, J. F.; Morrell, M. M.; Kippelen, B.; Peyghambarian, N. *Appl. Phys. Lett.* **1997**, *71*, 1762–1764.
(34) Li, F.; Tang, H.; Anderegg, J.; Shinar, J. *Appl. Phys. Lett.* **1997**, *70*, 1233–1235.
(35) Zhang, S. T.; Ding, X. M.; Zhao, J. M.; Shi, H. Z.; He, J.; Xiong, Z. H.; Ding, H. J.; Obbard, E. G.; Zhan, Y. Q.; Huang, W.; Hou, X. Y. *Appl. Phys. Lett.* **2004**, *84*, 425–427.
(36) Zhao, J. M.; Zhang, S. T.; Wang, X. J.; Zhan, Y. Q.; Wang, X. Z.; Zhong, G. Y.; Wang, Z. J.; Ding, X. M.; Huang, W.; Hou, X. Y. *Appl. Phys. Lett.* **2004**, *84*, 2913–2915.
(37) Choi, H. W.; Kim, S. Y.; Kim, W.-K.; Lee, J.-L. *Appl. Phys. Lett.* **2005**, *87*, 082102.
(38) Zhang, S. T.; Zhou, Y. C.; Zhao, J. M.; Zhan, Y. Q.; Wang, Z. J.; Wu, Y.; Ding, X. M.; Hou, X. Y. *Appl. Phys. Lett.* **2006**, *89*, 043502.
(39) Jin, Y. D.; Ding, X. B.; Reynaert, J.; Arkhipov, V. I.; Borghs, G.; Heremans, P. L.; Van der Auweraer, M. *Org. Electron.* **2004**, *5*, 271–281.
(40) Demirkan, K.; Mathew, A.; Weiland, C.; Yao, Y.; Rawlett, A. M.; Tour, J. M.; Opila, R. L. *J. Chem. Phys.* **2008**, *128*, 074705.
(41) Waser, R.; Aono, M. *Nat. Mater.* **2007**, *6*, 833–840.
(42) Choi, B. J.; Jeong, D. S.; Kim, S. K.; Rohde, C.; Choi, S.; Oh, J. H.; Kim, H. J.; Hwang, C. S.; Szot, K.; Waser, R.; Reichenberg, B.; Tiedke, S. *J. Appl. Phys* **2005**, *98*, 033715-1–033715-10.
(43) Yang, J. J.; Pickett, M. D.; Li, X.; Ohlberg, D.; Stewart, D.; Williams, R. S. *Nat. Nanotechnol.* **2008**, 429–433.
(44) Strukov, D. B.; Snider, G. S.; Stewart, D. R.; Williams, R. S. *Nature* **2008**, *453*, 80–83.
(45) Wu, J.; Mobley, K.; McCreery, R. *J. Chem. Phys.* **2007**, *126*, 24704.
(46) McCreery, R.; Wu, J.; Kalakodimi, R. J. *Phys. Chem. Chem. Phys.* **2006**, *8*, 2572–2590.
(47) Nowak, A.; McCreery, R. *J. Am. Chem. Soc.* **2004**, *126*, 16621–16631.
(48) Ranganathan, S.; McCreery, R.; Majji, S. M.; Madou, M. *J. Electrochem. Soc.* **2000**, *147*, 277–282.
(49) Ranganathan, S.; McCreery, R. L. *Anal. Chem.* **2001**, *73*, 893–900.
(50) Barbier, B.; Pinson, J.; Desarmot, G.; Sanchez, M. *J. Electrochem. Soc.* **1990**, *137*, 1757–1764.
(51) Deinhammer, R. S.; Ho, M.; Anderegg, J. W.; Porter, M. D. *Langmuir* **1994**, *10*, 1306–1313.
(52) Anariba, F.; DuVall, S. H.; McCreery, R. L. *Anal. Chem.* **2003**, *75*, 3837–3844.
(53) Kalakodimi, R. P.; Nowak, A. M.; McCreery, R. L. *Chem. Mater.* **2005**, *17*, 4939–4948.
(54) Anariba, F.; Steach, J. K.; McCreery, R. L. *J. Phys. Chem. B* **2005**, *109*, 11163–11172.
(55) McCreery, R.; Dieringer, J.; Solak, A. O.; Snyder, B.; Nowak, A. M.; McGovern, W. R.; DuVall, S. *J. Am. Chem. Soc.* **2003**, *125*, 10748–10758.
(56) McCreery, R. L.; Wu, J.; Kalakodimi, R. P. *Phys. Chem. Chem. Phys.* **2006**, *8*, 2572–2590.
(57) Hansen, W. N.; Hansen, G. J. *Surf. Sci.* **2001**, *481*, 172–184.
(58) Campbell, I. H.; Rubin, S.; Zawodzinski, T. A.; Kress, J. D.; Martin, R. L.; Smith, D. L.; Barashkov, N. N.; Ferraris, J. P. *Phys. Rev. B* **1996**, *54*, R14321.
(59) Alloway, D. M.; Hofmann, M.; Smith, D. L.; Gruhn, N. E.; Graham, A. L.; Colorado, R.; Wysocki, V. H.; Lee, T. R.; Lee, P. A.; Armstrong, N. R. *J. Phys. Chem. B* **2003**, *107*, 11690–11699.
(60) Giordano, L.; Cinquini, F.; Pacchioni, G. *Phys. Rev. B: Condens. Matter Mater. Phys.* **2006**, *73*, 045414/4–045414/6.
(61) Zehner, R. W.; Parsons, B. F.; Hsung, R. P.; Sita, L. R. *Langmuir* **1999**, *15*, 1121–1127.
(62) Wang, B.; Luo, J.; Wang, X.; Wang, H.; Hou, J. G. *Langmuir* **2004**, *20*, 5007–5012.
(63) Rampi, M. A.; Schueller, O. J. A.; Whitesides, G. M. *Appl. Phys. Lett.* **1998**, *72*.
(64) Porter, M. D.; Bright, T. B.; Allara, D. L.; Chidsey, C. E. D. *J. Am. Chem. Soc.* **1987**, *109*, 3559–3568.
(65) Brezna, W.; Fischer, M.; Wanzenboeck, H. D.; Bertagnolli, E.; Smoliner, J. *Appl. Phys. Lett.* **2006**, *88*, 122116.
(66) Green, M. L.; Sorsch, T. W.; Timp, G. L.; Muller, D. A.; Weir, B. E.; Silverman, P. J.; Moccio, S. V.; Kim, Y. O. *Microelectron. Eng.* **1999**, *48*, 25–30.
(67) Shamala, K. S.; Murthy, L. C. S.; Narasimha Rao, K. *Mater. Sci. Eng. B* **2004**, *106*, 269–274.
(68) Gusev, E. P.; Cartier, E.; Buchanan, D. A.; Gribelyuk, M.; Copel, M.; Okorn-Schmidt, H.; D'Emic, C. *Microelectron. Eng.* **2001**, *59*, 341–349.
(69) Voigt, M.; Sokolowski, M. *Mater. Sci. Eng. B* **2004**, *109*, 99–103.
(70) Groner, M. D.; Elam, J. W.; Fabreguette, F. H.; George, S. M. *Thin Solid Films* **2002**, *413*, 186–197.
(71) Rao, M. V.; Rajeshwar, K.; Verneker, V. R. P.; DuBow, J. *J. Phys. Chem* **1980**, *84*, 1987–1991.
(72) Mikhelashvili, V.; Eisenstein, G. *J. Appl. Phys.* **2001**, *89*, 3256–3269.
(73) Tao, N. J. *Phys. Rev. Lett.* **1996**, *76*, 4066.
(74) Tran, E.; Grave, C.; Whitesides, G. M.; Rampi, M. A. *Electrochim. Acta* **2005**, *50*, 4850–4856.
(75) Tran, E.; Duati, M.; Ferri, V.; Mullen, K.; Zharnikov, M.; Whitesides, G. M.; Rampi, M. A. *Adv. Mater.* **2006**, *18*, 1323–1328.
(76) Demkov, A. A.; Fonseca, L. R. C.; Verret, E.; Tomfohr, J.; Sankey, O. F. *Phys. Rev. B: Condens. Matter Mater. Phys.* **2005**, *71*, 195306.

AM800126V